Multifocal Raman spectrophotometer for examining drug-induced and chemical-induced cellular changes in 3D cell spheroids

Hao-Xiang Liao[1], Kazuki Bando[1,2], Menglu Li[1,2], Katsumasa Fujita[1,2,3]*

AFFILIATIONS

1 Department of Applied Physics, Osaka University, Suita, Osaka 565-0871, Japan

2 AIST Advanced Photonics and Biosensing Open Innovation Laboratory, Suita, Osaka 565-0871, Japan

3 Institute for Open and Transdisciplinary Research Initiatives, Suita, Osaka 565-0871, Japan

*Correspondence to: Katsumasa Fujita

EMAIL: fujita@ap.eng.osaka-u.ac.jp

ABSTRACT

Cell spheroids offer alternative *in vitro* cell models to monolayer cultured cells because they express complexities similar to those of *in vivo* tissues, such as cellular responses to drugs and chemicals. Raman spectroscopy emerged as a powerful analytical tool for detecting chemical changes in living cells because it non-destructively provides vibrational information regarding a target. Although multiple iterations are required in drug screening to determine drugs to treat cell spheroids and assess the inter-spheroid heterogeneity, current Raman applications used in analyzing spheroids enable the observation of only a few spheroids owing to the low throughput of Raman spectroscopy. In this study, we developed a multifocal Raman spectrophotometer that enables simultaneous analysis of multiple spheroids in separate wells of a regular 96-well plate. By utilizing 96 focal spots and parallel collection, our system can improve the throughput by approximately two orders of magnitude compared to the throughput of a conventional single-focus Raman microscope. The Raman spectra of HeLa cell spheroids treated with anticancer drugs and HepG2 cell spheroids treated with free fatty acids were measured simultaneously, and concentration-dependent cellular responses were observed in both studies. Using the multifocal Raman spectrophotometer, we rapidly observed chemical changes in spheroids, and thus this system can facilitate the application of Raman spectroscopy in analyzing the cellular responses of spheroids.

INTRODUCTION

In the last two decades, cell spheroids have increasingly been used as models in drug response[1-3] and toxicity studies[4-6] because they express intermediate complexities between those of two-dimensional (2D) monolayer cultured cells and *in vivo* tissues.[1-6] Spheroids exhibit higher resistance to drugs and chemicals than those of 2D monolayer cultured cells due to the penetration depth of the chemical and the cell-cell and cell-extracellular matrix interactions within the spheroids.[1-3] For example, compared to 2D cultured tumor and hepatocyte cells, tumor and hepatocyte spheroids display higher drug[1-3] and steatosis resistances,[4, 5] respectively. Therefore, cell spheroids offer more accurate models that reflect *in vivo* cell-chemical interactions.

Although the spheroid model bridges the gap between traditional 2D models and *in vivo* tissues, the tools used to screen for chemical changes in spheroids exhibit advantages and limitations.[7, 8] For example, the polymerase chain reaction[9, 10] and gel electrophoresis (comet) assays,[11, 12] which enable detailed analyses of gene and protein compositions, are destructive methods that lyse spheroids to extract the genes and proteins. Techniques such as fluorescence assays[7, 8, 13] and colorimetric assays[7, 8, 14] enable the observation of specific components within cells, the structures of spheroids, or cell viability using dyes, but the incorporation of dyes may alter the biochemical properties of the target. These methods require sacrificing spheroids or measuring at endpoints, rendering their combination with other analytical techniques for further analysis challenging. Non-invasive methods such as scanning electrochemical microscopy can assess the specific redox activities within cells,[15, 16] and optical microscopy can observe the growth and morphologies of spheroids.[7, 8] Since these methods provide partial information regarding spheroid conditions, combining them with a compositional analysis is necessary to understand the mechanisms of cell-chemical interactions.

Raman spectroscopy emerged as a powerful analytical tool for studying living cells because it non-destructively assesses fingerprint-like features of vibrational information and requires minimal sample preparation.[17-20] Raman spectroscopy has been used to study 2D cellular models, including those of cell-drug interactions[21, 22] and cellular changes during steatosis,[23, 24] but its low throughput limits its applications in examining spheroids, and only a few studies have been reported.[25-29] Jamieson et al. used Raman imaging to study the responses of tumor spheroids to anticancer drug therapy, demonstrating the potential of Raman spectroscopy in examining heterogeneities within and across spheroids.[27] Jung et al. reported a proof-of-concept study to improve the throughput by collecting the averaged signals of whole organoids and successfully studied over one hundred organoids under the same conditions.[29]

To facilitate pharmaceutical applications, improving the throughput of Raman measurements is

required to examine spheroids under different treatment conditions[30, 31] and assess the heterogeneity among spheroids.[8, 32, 33] Recently, Raman systems equipped with parallel excitation and signal acquisition emerged to improve the throughput of Raman spectroscopy. Two multifocal Raman systems have been developed to simultaneously observe multiple samples under various conditions.[34-36] Our previous attempt used a lens array and large-area illumination to simultaneously measure 192 wells in a 384-well plate by irradiating the wells with a truncated enlarged Gaussian beam.[34] However, the truncation and beam splitting resulted in a non-uniform excitation power, with a six-fold difference between the wells, which could cause non-uniform signal levels and different laser-induced biological effects in cell samples.[34] Another approach employed a diffractive optical element to realize beam splitting.[35, 36] This parallelized Raman system simultaneously detected the Raman signals of 64 wells in a 1536-well plate with a uniform illumination power over the samples and a collection numerical aperture (NA) of 0.14.[35, 36]

In this study, we aimed to provide rapid Raman analyses of spheroids in 96-well plates, a common format employed for culturing and screening spheroids. We developed a multifocal Raman spectrophotometer for detecting chemical changes in spheroids. An optical system was designed to illuminate 96 wells, with a uniform laser power and high collection NA (0.5). As a demonstration of parallel Raman performance, we measured 96 different crystalline samples in approximately 2 minutes. In terms of spheroid measurements, we simultaneously observed the Raman spectra of multiple drug-treated tumor spheroids and free fatty acid (FFA)-treated hepatocyte spheroids at various treatment concentrations. Concentration-dependent cellular responses of spheroids were observed, and > 100 spheroids were measured, indicating that the developed system displays the potential to facilitate the application of Raman spectroscopy to drug and chemical responses in 3D cell spheroids.

RESULTS

Multifocal Raman spectrophotometer for use in the rapid examination of spheroids under various conditions

We developed a multifocal Raman spectrophotometer for parallel Raman measurements of spheroids in a regular 96-well plate, with a uniform excitation power and similar signal collection efficiencies between the wells. It contains a fiber-based laser introduction system with a laser power compensation mechanism to introduce the laser to the dichroic mirror (DM) mount (Figure 1B), where a set of reflection-ratio-designed DMs divides the laser beam. Two lens arrays focus the resulting laser beams to target the spheroids and collect their Raman signals, and an optical fiber array delivers the collected Raman signals to an imaging spectrophotometer (Figure 1A).

In the fiber-based laser introduction system (Figure 1B), a single laser beam is split into six beams using commercial beam splitters, which are then further split into 24 beams via 1-to-4 fiber splitters. These beams are delivered to the entrances on both sides of the DM mount, as shown in Figure 1A. The differences in the laser powers of the six divided beams are compensated by tuning the optical alignment of each incident laser beam to ensure that the laser powers at the fiber splitter output are similar. Thus, 24 uniform laser beams (beam width: 4.3 mm (full width at $1/e^2$) can be provided at each entrance of the DM mount. In the DM mount, each beam is split into four beams via four DMs with reflection efficiencies of 25%, 33%, 50%, and 100% and focused using a lens array (effective excitation NA = 0.27) to generate 96 focal spots in total (Figure 1A). These designs provide a more uniform excitation power to the 96 samples, with less loss of laser power (13.4 ± 1.1 mW using a 4 W continuous wave (CW) laser) compared to that in our previous study[34] (192 focal spots with a laser power of 6.0 ± 2.2 mW using a 15 W CW laser). The excitation power exhibits a standard deviation (SD) of 8%, which is mainly due to the mismatch of the designed and real reflection efficiencies of the DMs.

The optical system to achieve parallel detection employs a design similar to that used in our previous study.[34] Raman scattering from the samples is collected (effective collection NA = 0.5) individually via the same lens array and introduced into an optical fiber array with an outlet aligned with the entrance slit of the spectrometer. The spectrophotometer disperses the Raman signal from each well onto a 2D charge-coupled device (CCD) camera. The pitch of the fiber array and fiber core size are set to 200 and 105 μm, respectively, to avoid crosstalk of Raman signals between adjacent wells.

Figure S1 shows the measured raw spectra of ethanol (EtOH) in a 96-well plate, where the 96 bright stripes represent the Raman spectra from the corresponding wells. The intensities of the detected

EtOH signals are comparable to that measured using a single-focus confocal Raman microscope with NA-0.45 objective, excitation power of 13 mW at 532 nm, confocal aperture of 1 Airy unit (AU), same diffraction grating, CCD camera, and exposure time. The SD of the Raman signals across the wells was 16%, suggesting comparable signal-to-noise ratios. The EtOH Raman signals were used as a reference for intensity calibration across the wells in the other experiments in this study.

In order to obtain the average Raman signal from different spheroids, the system is equipped with a motorized XYZ stage for scanning the 96-well plate in the lateral direction. The SD of the Raman signal of a homogeneous sample (evaluated using EtOH) measured at different locations in a well was 1%. The lateral resolution of the system was approximately 15 μm (full width at $1/e^2$), as confirmed by laterally scanning a 1 μm fluorescence bead. An axial resolution of approximately 270 μm (full width at half maximum) was confirmed by axially scanning through a rhodamine 6G film (<1 μm thickness) oriented orthogonally to the axis. This collection volume enabled the detection of only one spheroid in each exposure. Therefore, an average Raman signal from different spheroids in the same well can be obtained to study inter-spheroid heterogeneity.

To confirm that the multifocal Raman spectrophotometer can spectrally differentiate samples, we measured drug crystals. Figure 2A shows 96 Raman spectra of different samples (Figure S2 shows the layout), including the initial and anti-solvent recrystallized crystal (IC and RC) of four drug molecules in four solvent and anti-solvent combinations. Complete Raman spectra detected from individual wells are shown in Figures S3–S4. The characteristic Raman bands of each crystal form were measured (Figure S5) and assigned based on previous studies (Table S1).[37-42] The Raman bands of IC and RC indicate that they are different forms (Figure 2B). The result also indicates that the system can distinguish the shifts of the Raman peaks at a resolution of approximately one pixel (~ 3 cm^{-1}), although the signal is delivered by the optical fibers with a core size of approximately five pixels on the camera. The peak positions of the four Raman spectra of IC and RC around 1160 cm^{-1} (Figure 2C) are 1163.79 ± 0.28 and 1160.25 ± 0.69 cm^{-1}, respectively, calculated by Gaussian fitting after removing the background of the spectra using linear subtraction.

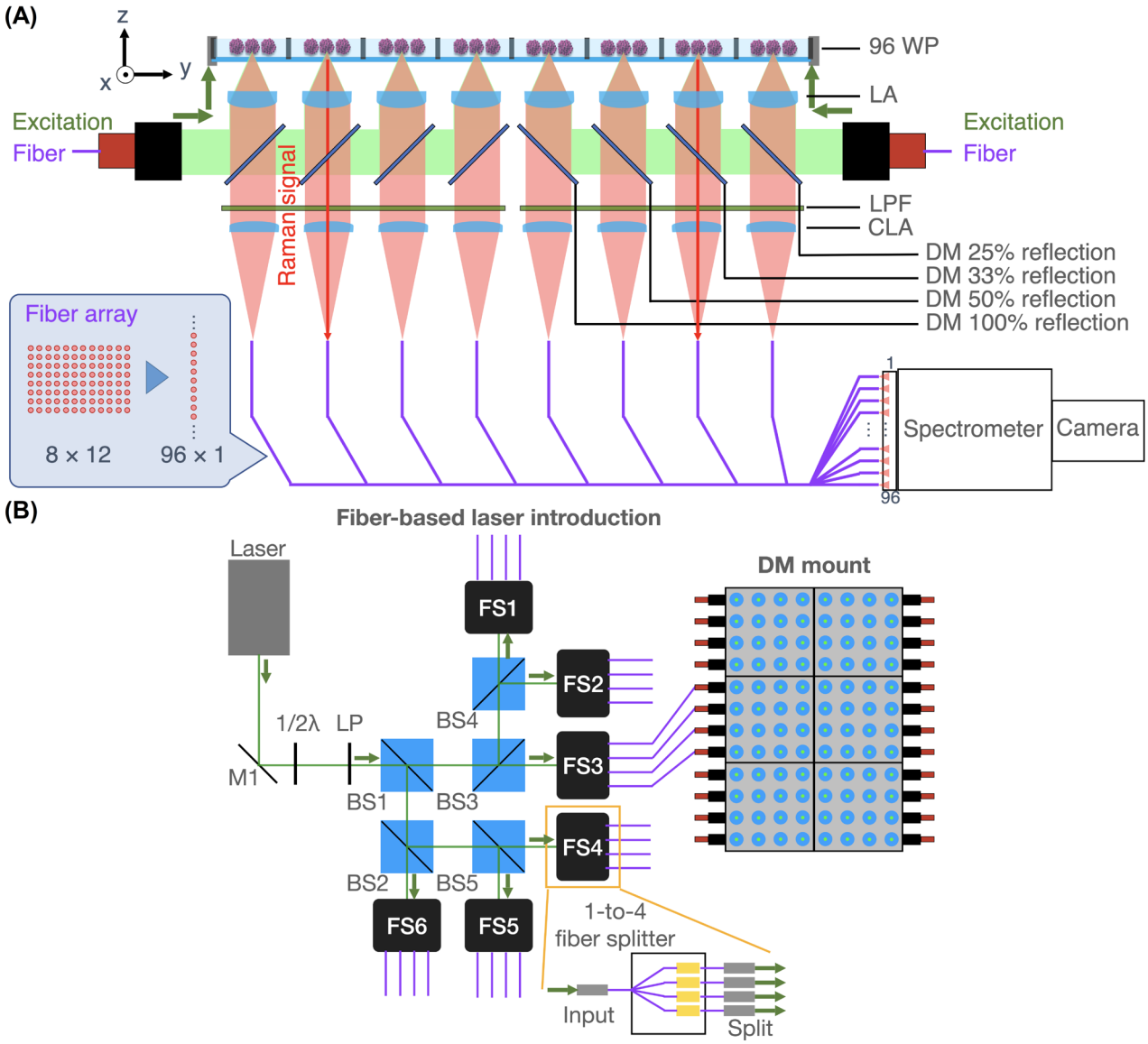

Figure 1. Multifocal Raman spectrophotometer for use in parallel Raman measurements of analytes in a 96-well plate. (A) Schematic diagram of the illumination and detection optics of the DM mount. The reflection efficiencies of the DMs were set to 25%, 33%, 50%, and 100% to split the laser beam uniformly. (B) Schematic diagram of the fiber-based laser introduction system. BSs and FSs split one laser beam into 24 beams incident into the side of (A), the DM mount. WP: well plate; LA: lens array; LPF: long pass filter; CLA: coupling lens array; DM: dichroic mirror; LP: linear polarizer; BS: beam splitter; FS: 1-to-4 fiber splitter.

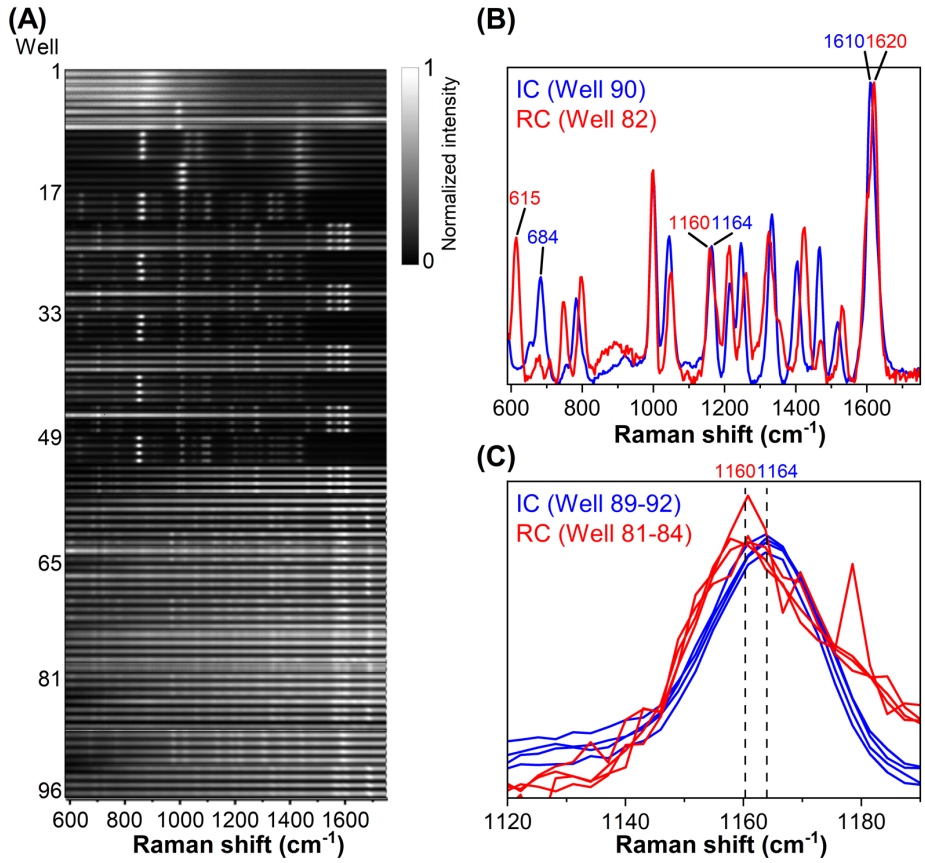

Figure 2. Parallel Raman measurements of 96 different samples containing four types of small-molecule drug crystals that were recrystallized under various conditions. Complete information regarding the samples is available in the supporting information. (A) Raman spectra of the 96 different samples, which the intensity of each Raman spectrum was normalized by dividing by the maximum intensity calculated after subtracting the minimum intensity in the spectrum. Representative Raman spectra of the (B) initial and recrystallized crystal (IC and RC) in one well in the spectral range 590–1750 cm^{-1} and the (C) ICs and RCs in four wells in the spectral range 1120–1190 cm^{-1}.

Sample preparation for multifocal Raman measurement

Spheroids treated with various concentrations of chemicals were prepared, and spheroid culturing is described in the "METHODS AND MATERIALS" section. For Raman measurement, the treated spheroids were transferred into a glass-bottom 96-well plate with Raman scattering that did not interfere with the Raman peaks of interest: those of cytochromes, lipids, and drugs. The culture medium was replaced with Hank's balanced salt solution (HBSS) to reduce background fluorescence from the culture medium, drugs, and FFAs. To maximize the collection volume within the spheroid and to avoid background signals from the glass substrate, the spheroid was grown to approximately the size of the axial resolution (270 μm) and the laser beams were focused on the center of the spheroid. Raman measurements were performed by scanning the plate at 400 μm intervals to collect Raman signals from different spheroids.

Rapid Raman observation of the dose-dependent drug effects in cancer-cell spheroids

Although Raman spectroscopy is used to assist in understanding the effects of drugs on spheroids,[27] its application to drug-treated spheroids remains limited to low-throughput observations. Herein, the multifocal Raman spectrophotometer was applied to observe the cellular responses in the drug-treated spheroids. The Raman spectra of spheroids treated with various drug concentrations in different wells were measured simultaneously, and dose-dependent chemical changes in the spheroids were observed.

The drug responses of HeLa spheroids treated with various concentrations of actinomycin D (ActD) solutions were studied. ActD is the first antibiotic proven to work as an anticancer drug, which binds to DNA and inhibits RNA transcription in cancer cells.[43] HeLa spheroids were cultured in a micropatterned plate, transferred into a 96-well plate, and then treated with 0–10 μM ActD for eight hours. Six ActD concentrations were prepared in 12 wells, with two wells for each concentration. After washing the medium containing the drugs, Raman spectra were measured at 24 positions in each well. The data obtained at positions with no cell signals, as determined using the Raman intensity of CH_3 (2936 cm^{-1}), were excluded from the subsequent analysis.

Figure 3A shows the mean Raman spectra of ActD-treated HeLa spheroids. Baseline removal via polynomial fitting was performed to remove the fluorescence from ActD. Despite the high shot noise due to the strong fluorescence of ActD, a decrease in the Raman intensity at 1585 cm^{-1}, which can be assigned to cytochrome *c* (cyt *c*),[44, 45] is observed. This result indicates possible cytotoxicity after ActD treatment, which is consistent with the results of a previous studies.[21, 45] The increase in the Raman intensity at 1485 cm^{-1}, which can be assigned to ActD, indicates the uptake of ActD by the spheroid.

A significant decrease in I_{1585} is observed at ActD concentrations of 0.3 to 10 μM and a significant

increase in I_{1485} is observed at ActD concentrations of 1 to 10 μM (Figures 3B and 3C). For the comparison among different conditions, the area of the Raman peak of CH_3 (2936 cm^{-1}) is used as a reference to indicate the detected volume in spheroids. We also conducted an ATP assay to assess the cytotoxicity of ActD treatment on HeLa spheroids (Figure S6). The relation of cell viability and ActD concentrations is consistent with the decrease of Raman intensities of 1585 cm^{-1}. In ActD-treated 2D cultured HeLa cells in the previous study,[21] the decrease in the cyt *c* signal was observed after 0.1 μM ActD treatment for the same duration. This result suggests that 3D spheroids are more resistant to drug treatment than 2D cultured cells. Our system exhibits the potential to rapidly screen for dose-dependent drug effects in 3D spheroids, thereby facilitating Raman studies of 3D spheroids in the field of drug development.

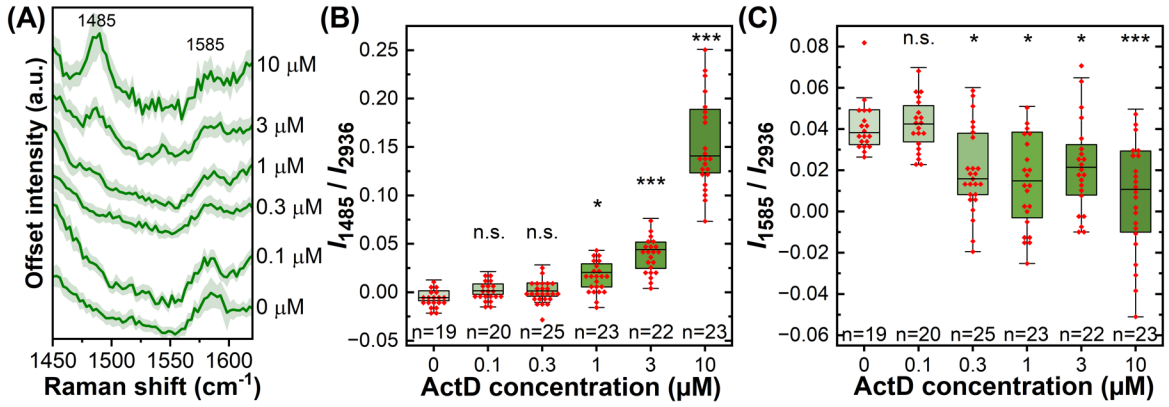

Figure 3. Raman observation of the drug effect of HeLa spheroids under a range of drug concentrations treatment (0–10 μM). (A) Raman spectra of ActD-treated HeLa spheroids. The solid lines indicate the mean values, and the standard deviations are shown in light green. The boxplots of the Raman intensities at (B) 1485 (assigned to ActD) and (C) 1585 cm^{-1} (assigned to cyt *c*) normalized by dividing by 2936 cm^{-1} (as reference for detected volume in spheroids) reveal a dose-dependent intensities change. The boxplots illustrate the internal data points (center line: median, box: quartiles, low/up whiskers: max/min value in 1.5 interquartile range). Significant difference was compared with the leftmost box. ***: $P < 0.001$; *: $P < 0.05$; n.s.: $P > 0.05$.

Rapid and quantitative Raman observation of FFA-induced effects in hepatocyte spheroids

Non-alcoholic fatty liver disease (NAFLD), which is a common liver disease, was selected as another target. NAFLD is associated with excessive uptake of FFAs, with 2 mM FFA reported to be cytotoxic to HepG2 cells, as determined via a cell viability assay.[46] Raman spectroscopy has also been used to study the chemical changes in hepatocytes after exposed to excess FFAs.[23, 47] However, the relationship between the FFA concentrations and Raman spectra of hepatocyte spheroids has not been studied quantitatively. Herein, we demonstrated the rapid Raman observation of FFA-concentration-dependent chemical changes in hepatocyte spheroids using the multifocal Raman spectrophotometer.

HepG2 spheroids were treated with 0–2.0 mM concentrations of FFA for two days and then rinsed prior to Raman measurement. Seven FFA concentrations were prepared in 14 wells, with two wells for each concentration. Raman spectra were measured at 24 positions in each well, and the data obtained at the positions with no cell signals, as determined using the Raman intensity of CH_3 (2936 cm^{-1}), were excluded from the subsequent analysis.

Figure 4A shows the baseline-subtracted Raman spectra of HepG2 spheroids treated with various concentrations of FFAs. Decreases in the Raman intensities at 750, and 1585 cm^{-1}, which can be assigned to cytochromes, are observed, suggesting the oxidation of cytochromes by the FFAs or damage to the mitochondria due to the high concentrations of FFAs.[23] An increase in the Raman intensity 1445, 2850, and 2855 cm^{-1}, which can be assigned to lipid, are observed, indicating the accumulation of lipids in the hepatocytes. The change in Raman intensity at 1000 cm^{-1} (the # in Figure 4A) is not attributed to cellular changes but rather to the well plate pre-coated using collagen, which I_{1000} exhibits varying strengths at different locations within a well without cells (Figure S8).

The relationships between the FFA concentrations and Raman intensities assigned to the lipids and cytochromes are shown in boxplots (Figures 4B and 4C). For the statistical analysis, the intensity at 1680 cm^{-1} (assigned to amide-I), which does not correlate significantly with FFA concentration, is used as the reference for the detected volume in spheroids. The intensity at 750 cm^{-1}, which is the highest intensity among the Raman peaks assigned to cytochromes, is used to represent the cytochrome signal. A positive correlation between the intensity at 1445 cm^{-1} and FFA concentration is observed, indicating FFA-concentration-dependent lipid accumulation in the hepatocytes. The intensity at 750 cm^{-1} decreases and show significant difference under 2 mM FFA concentration. In the ATP assay result (Figure S7), the cell viability also decreased significantly when the HepG2 spheroid exposes to 2 mM FFA, consistent to the Raman observations result. Using the multifocal Raman spectrophotometer, we demonstrated the rapid Raman observation of concentration-dependent chemical changes in hepatocyte spheroids exposed to FFAs. Therefore, the system can be a tool for rapidly screening

chemical compounds that induce mitochondrial toxicity.

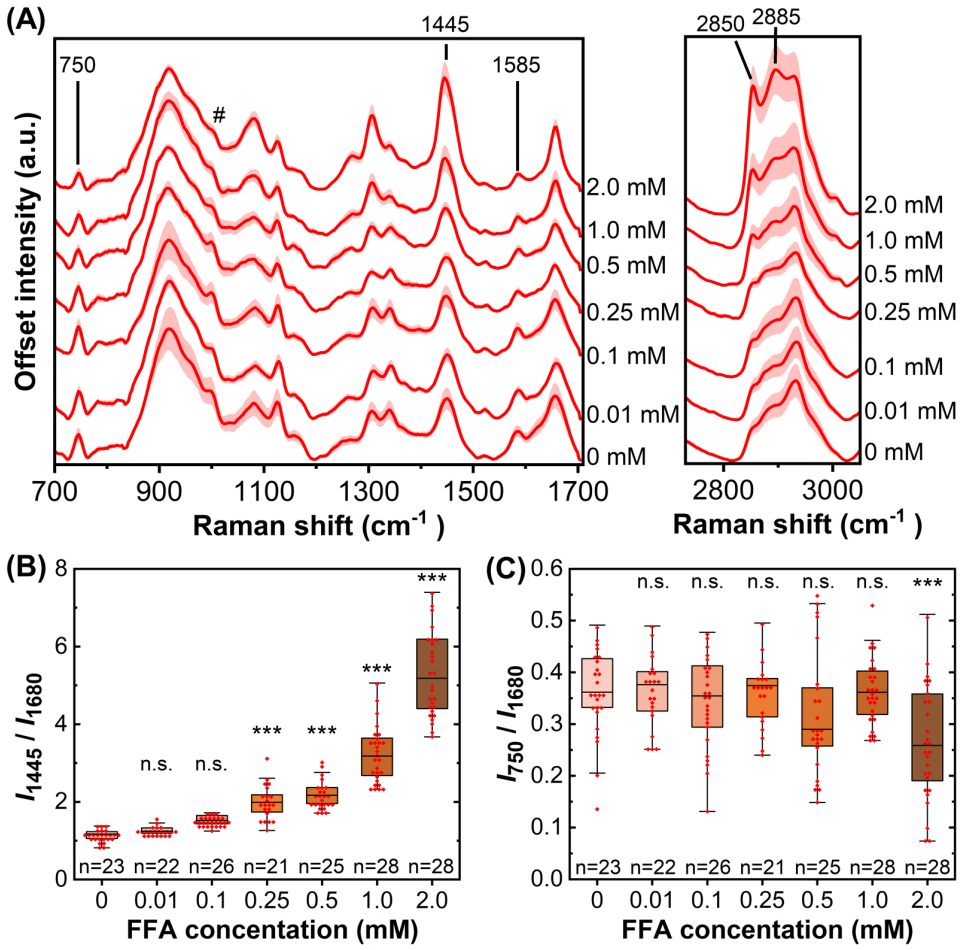

Figure 4. Parallel Raman observations of lipid accumulation and overloading of FFA in HepG2 spheroids under various FFA concentrations treatment (0–2 mM). (A) Fingerprint and CH regions of the Raman spectra of the FFA-treated HepG2 spheroids. The solid lines indicate the mean values, and the standard deviations are shown in light red. The boxplots of the normalized Raman intensities at (B) 1445 (assigned to lipid) and (C) 750 cm^{-1} (assigned to cytochrome) reveal a concentration-dependent intensities change. The boxplots illustrate internal data points. (center line: median, box: quartiles, low/up whiskers: max/min value in 1.5 interquartile range). Significant difference was compared with the leftmost box. ***: $P < 0.001$; n.s.: $P > 0.05$.

DISCUSSIONS

In this study, we developed a multifocal Raman spectrophotometer for use in the simultaneous Raman observations of chemical changes in multiple 3D cell spheroids at uniform excitation power and signal levels in a 96-well plate. We simultaneously measured 96 wells containing different crystalline samples in 126 seconds, whereas a single-focus Raman system requires at least 3.4 hours to perform these measurements under the same exposure condition, excluding the time required to scan the plate. We also examined HeLa spheroids treated with various doses of ActD in 12 wells and HepG2 spheroids treated with different FFA concentrations in 14 wells. We rapidly assessed > 100 spheroids and observed dose-concentration-dependent cellular changes in both studies. Although increasing the excitation power can also accelerate signal collection in a single focus system, high laser power may induce photodamage in the cell sample. In contrast, the parallel measurement improves the throughput without increasing the laser power, which also eliminates the necessity to travel between wells, resulting in the significant reduction of measurement time. Note that for spheroid measurements, we only used 12 and 14 wells of HeLa and HepG2 spheroids for the measurements, not due to the limitations of the developed system, but due to the need for a large number of spheroids. The developed system can observe 96 wells simultaneously. When combined with a mass culture system and an automated sample dispensing system, the system can be used for more efficient screening.

We designed the system to measure relatively thick samples, such as cell spheroids, solutions, and powders. To collect an averaged Raman signal of a spheroid (250–300 μm in diameter), we utilized an excitation NA (0.27) smaller than the collection NA (0.5) to yield a larger excitation volume and a confocal aperture size of approximately 20 AU to collect signals at a thickness of approximately 270 μm (full width at half maximum for axial resolution). Therefore, when observing thin samples, poor axial resolution can result in a significant background signal from the out-of-focus planes, such as the substrate and medium, which may obscure the small Raman signal.

The Raman spectra of the ActD-treated HeLa spheroids (Figure 3) suggest uptake of the anticancer drug and damage to the cells. The Raman spectra of FFA-treated HepG2 spheroids indicate that the accumulation of FFA in hepatocytes was quantitatively observed (Figure 4). These results reveal the effectiveness of the developed system in observing the cellular responses in spheroids, the potential of the system for use in high-throughput screening of drug responses, and the effects of chemicals on 3D cell spheroids.

Raman spectroscopy is generally used to visualize the chemical distributions or trace drug delivery within spheroids.[27, 28] However, identifying the Raman measurement conditions, optimizing the concentration ranges of drugs, and establishing the inter-spheroid heterogeneities of drug effects are

extremely time-consuming. As the multifocal Raman spectrophotometer can efficiently measure multiple spheroids under various treatment conditions, the system can be used as a pre-screening method to reduce time consumption.

As the multifocal Raman spectrophotometer can be used in parallel measurements of the Raman spectra of liquid, solid, and cell samples under various conditions, the system should also contribute to improving efficiency in the pharmaceutical and biochemical fields. Parallel time-series Raman observations are useful in observing chemical reaction kinetics, including continuous crystallization and aging of packaged drugs, in addition to cell activities, such as cell differentiation and metabolism. To further probe specific chemical reactions, utilizing an alkyne tag or deuterated compounds may be an option for optimization.[48, 49] Surface-enhanced Raman spectroscopy is also possible using this system, which may further improve the throughput of Raman screening.[50] The fiber-based laser introduction and signal delivery within the multifocal Raman spectrophotometer render the system flexible and compact. The excitation and collection parts (the DM mount) have compact dimensions (≈ 13 × 11 × 6 cm), rendering the integration of the system into another system as an inline quality control system simple.

METHODS AND MATERIALS

Optical design

A 532 nm CW laser (opus 532, Laser Quantum) is used as a light source with a 4 W laser output (Figure 1B). Beam splitters (BS1–BS5, 50:50 and 30:70 beam splitters, Thorlabs) and 1-to-4 fiber splitters (customized, TATSUTA Electric Wire & Cable) are used to split the laser beam into 24 Gaussian beams and direct them to the DM mount. A set of DMs with reflection efficiencies of 25%, 33%, 50%, and 100% (Figure 1A, customized, Asahi Spectra) are used to split the 24 beams into 96 beams, and then a lens array (47-460, Edmund Optics) focuses the beams to excite the samples in a 96-well plate. A glass-bottom 96-well plate (GP96000, Matsunami Glass) is placed on a holder equipped with a motorized XY stage (Opto-Sigma) and Z stage (Chuo Seiki) to move the well plate. The average excitation power over the 96 wells is 13.4 mW for Figures 3 and 4 and 12 mW for Figure 2. A fiber array (FG105LVA, Thorlabs) is used to align the Raman signal collected by the coupling lens arrays from 8 × 12 to 96 × 1 to couple it to a spectrometer (Isoplane 320 advanced, Teledyne Princeton Instruments). Raman spectra are collected using a 2D cooled CCD camera (PIXIS 400B eXcelon, Teledyne Princeton Instruments), and 400 pixels of the camera are used to resolve the spectrum. A grating with 600 grooves/mm blazed at 500 nm is used for the spectral range 590–1750 or 2500–3430 cm^{-1}, with a spectral interval of approximately 2.9 or 2.5 cm^{-1}/pixel, respectively.

Raman measurement

The Raman measurements of recrystallized crystals (Figure 2) were performed at nine positions in the well. The total measurement time was 126 seconds, including a camera readout time of 36 seconds. The Raman measurements of spheroids were performed at 24 positions in the well, with total measurement times of 1.65 hours. The Raman measurements of spheroids were performed in two spectral ranges, 2500–3440 cm^{-1} and then 590–1750 cm^{-1}, with 120 seconds laser exposure for each spectral range, at the same position.

Drug recrystallization

Four types of drugs, i.e., mannitol (99%, Sigma-Aldrich), carbamazepine (97%, FUJIFILM Wako Pure Chemical Corporation), flufenamic acid (97%, Sigma-Aldrich), and indomethacin (98%, Tokyo Chemical Industry), and three types of solvents, i.e., EtOH (99.5%, FUJIFILM Wako Pure Chemical Corporation), methanol (99.8%, FUJIFILM Wako Pure Chemical Corporation), and H_2O (Milli-Q water), were used. Following the layout shown in Figure S2, the drug powder and solvent are added to each well to form 100 μL saturated solutions at 25°C. After the drug powder is dissolved, 50 or 100 μL of anti-solvent is added instantaneously, and the plate is placed in an oven at 70°C overnight to dry.

3D Cell spheroid culture for Raman observation

HeLa cells were seeded into a micropatterned 6-well plate (4810-900SP, Iwaki) at a seeding density of 100 cells/chamber to form cell spheroids. The cells were then maintained in minimum essential medium (MEM, 51200038, Thermo Fisher Scientific) supplemented with 10% fetal bovine serum (10270106, Thermo Fisher Scientific), penicillin-streptomycin-glutamine (100 U/mL penicillin G, 100 μg/mL streptomycin, 292 μg/mL L-glutamine; 10378016, Thermo Fisher Scientific), 1% MEM non-essential amino acids solution (11140050, Thermo Fisher Scientific), and 20 mM HEPES buffer (H0887, Sigma Aldrich) in an atmosphere of 5% CO_2 at 37°C. After four days of culturing with daily medium changes, HeLa spheroids with diameters of 250–300 μm were formed. The spheroids were then transferred to a 96-well plate, which was pre-coated with 0.01% collagen type I solution (IFP9660, Research Institute for the Functional Peptides) overnight at room temperature, with a density of several hundred spheroids per well. The spheroids were treated by 0–10 μM ActD solutions (010-21263, FUJIFILM Wako Pure Chemical Corporation) in culture medium containing 0.1% DMSO, with two wells used for each condition, followed by incubation for eight hours. Prior to the Raman measurements, the spheroids were rinsed several times with Dulbecco's phosphate buffered saline

solution (PBS solution; T900, Takara Bio), and then was replaced by HBSS (082-08961, FUJIFILM Wako Pure Chemical Corporation). Two wells of HBSS were prepared as no cells references.

HepG2 spheroids were prepared similarly to HeLa spheroids using the same seeding density and culturing time, but the culture medium did not contain HEPES buffer. On day 2 and day 3, FFA solutions were provided to the HepG2 spheroids to form final concentration 0–2 mM FFA solutions. The FFA solutions were formulated by dissolving palmitic acid (P9767, Sigma-Aldrich) and oleic acid (O7501, Sigma-Aldrich) in a mole ratio of 1:2 into culture medium containing 0.2 mM FFAs-free BSA. HepG2 under each condition were collected and seeded into a 96-well plate pre-coated using collagen, with two wells used for each condition. Prior to Raman measurement, the well plate was incubated for an hour to allow the spheroids to attach to the collagen-coated surface, and then the medium was replaced with HBSS.

ATP assay

An ATP assay kit for 3D spheroids (G9683, Promega) was utilized to assess the cell viability according to the protocol provided by the manufacturer. HeLa spheroids were prepared with a 96 wells low cell adhesion U bottom plate (MS-9096U, Sumitomo bakelite), and eight wells were used for each condition. We prepare a single spheroid in each well of a U bottom plate to yield a consistent spheroid number in each well. The seeding density was 100 cells/well with same total volume of culture medium in the well, and the incubation conditions was same as the spheroids used in Raman measurements. After treating HeLa spheroids with ActD solutions for eight hours, the samples and ATP assay reagents were placed in ambient for 30 minutes to equilibrate to room temperature (25ºC). Then, 30 μL of ATP assay reagent was added to each well, followed by mixing the samples on an orbital shaker for 5 minutes and leaving at room temperature for 25 minutes. Afterward, 50 μL of the solutions was transferred to a glass-bottom 96-well plate and their luminescence was evaluated using a microplate reader (Synergy HTX; BioTek). The cell viability was calculated as the luminescence value relative to the control. The procedure of ATP assay for FFA-treated HepG2 spheroids is similar to that for HeLa spheroids, except the FFA treatment time was two days.

Raman spectra data analysis

Spectral calibration of each well was performed using a spectral calibration lamp (6032, Newport) and the Raman peaks of EtOH. The Raman peak height of EtOH ($I_{2929} - I_{2550}$) were used as a reference to calibrate the intensity differences between the wells.

The data points with no cell signals, as determined using the height of the Raman peak at 2936 cm^{-1}

(I_{2936} - I_{3000}) were excluded from the data analysis of the results of the drug-treated and FFA-treated spheroids. The Raman spectra shown in Figure 2 B–C, Figure 3A, and Figure 4A were the averaged spectra after applying baseline correction via polynomial fitting to remove the fluorescence background. The peak intensities estimation process is shown in Figure S9. To estimate the intensities of the Raman peaks in the noisy Raman spectra in Figure 3, a three-point moving average is applied to smoothen each spectrum and a second-order polynomial baseline correction is conducted in the region around the Raman peaks. Following the baseline correction, the peak intensity is defined as the accumulation of the intensity around the Raman peaks at 1485 and 1585 cm^{-1} calculated after subtracting a linear baseline. The peak intensity estimation method used in Figure 4 was similar to Figure 3 but without the step of the polynomial baseline correction. To compare the Raman signals across different conditions, the Raman intensity was divided by the Raman intensity of the protein detected in the spheroids. The average intensity in 2934–2939 (assigned to CH_3 band of protein, indicated as I_{2936}) and 1672–1697 cm^{-1} (assigned to amide-I band of protein, indicated as I_{1680}), which were calculated after applying a three-point moving average and removing the baseline using linear subtraction, were used as a reference for detected volume in spheroids in Figure 3 and 4, respectively.

Statistical analysis

Statistical analysis was assessed with a one-way analysis of variance (one-way ANOVA), and individual differences were evaluated using the Tukey-Kramer's range tests for unequal sample sizes. All statistical analyses were performed using OriginLab 2022 (Learning Edition, Origin Lab Corporation). Statistical significance was set at $P < 0.05$. Symbols used are ***: $P < 0.001$; **: $P < 0.01$; *: $P < 0.05$; n.s. (not significant): $P > 0.05$.

ASSOCIATED CONTENT

Supporting Information

The Supporting Information is available free of charge at ACS Publication website.

The 96 Raman spectra of EtOH; layout of drug crystal recrystallization samples in the 96-well plate and the Raman spectra of these samples; Raman spectra of each crystal form of the four drug molecules and their Raman bands assignment; ATP assays of ActD-treated HeLa spheroids and FFA-treated HepG2 spheroids; Raman spectra of a well plate pre-coated using collagen; peak intensity estimation process (PDF)

AUTHOR INFORMATION

Corresponding Authors

Katsumasa Fujita – Department of Applied Physics, Osaka University, 2-1 Yamadaoka, Suita, Osaka 565-0871, Japan; AIST-Osaka University Advanced Photonics and Biosensing Open Innovation Laboratory, National Institute of Advanced Industrial Science and Technology (AIST), Suita, Osaka 565-0871, Japan; Email: fujita@ap.eng.osaka-u.ac.jp

Authors

Hao-Xiang Liao − Department of Applied Physics, Osaka University, Suita, Osaka 565-0871, Japan

Kazuki Bando – Department of Applied Physics, Osaka University, 2-1 Yamadaoka, Suita, Osaka 565-0871, Japan; AIST-Osaka University Advanced Photonics and Biosensing Open Innovation Laboratory, National Institute of Advanced Industrial Science and Technology (AIST), Suita, Osaka 565-0871, Japan;

Menglu Li − Department of Applied Physics, Osaka University, 2-1 Yamadaoka, Suita, Osaka 565-0871, Japan; AIST-Osaka University Advanced Photonics and Biosensing Open Innovation Laboratory, National Institute of Advanced Industrial Science and Technology (AIST), Suita, Osaka 565-0871

Author contributions: H.-X.L., B.K., and K.F. designed the system; H.-X.L., B.K., M.L., and K.F. designed the experiments; H.-X.L. and B.K. assembled the system; H.-X.L. and M.L. prepared the samples; H.-X.L. performed the experiments; H.-X.L., B.K., and M.L. analyzed the data; H.-X.L, B.K., M.L., and K.F. wrote the manuscript. All authors have read and agreed to the published version of the manuscript.

Notes: K. B. and K.F. applied a patent of multi-well Raman spectrophotometer. H.-X. L. and M. L. declare no potential conflict of interest.

ACKNOWLEDGMENT

We thank H. Kawagoe, T. Kubo, Y. Kumamoto, A. Nakayama, N. I. Smith, and K. Temma for discussions and comments. This research was supported by Osaka University Innovation Bridge Grant and JST COI-NEXT under Grant Number JPMJPF2009. The experiment was conducted at the Osaka University Photonics Center.

Table of contents

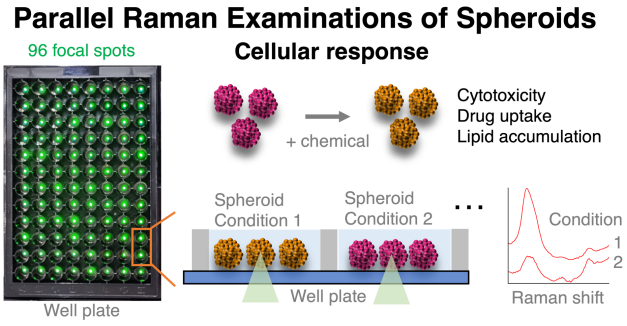

REFERENCES

1. Friedrich, J.; Seidel, C.; Ebner, R.; Kunz-Schughart, L. A., Spheroid-based drug screen: considerations and practical approach. *Nat. protoc.* **2009,** *4* (3), 309-324.
2. Mehta, G.; Hsiao, A. Y.; Ingram, M.; Luker, G. D.; Takayama, S., Opportunities and challenges for use of tumor spheroids as models to test drug delivery and efficacy. *J. Controlled Release* **2012,** *164* (2), 192-204.
3. Astashkina, A.; Grainger, D. W., Critical analysis of 3-D organoid in vitro cell culture models for high-throughput drug candidate toxicity assessments. *Adv. Drug Delivery Rev.* **2014,** *69-70*, 1-18.
4. van Grunsven, L. A., 3D in vitro models of liver fibrosis. *Adv. Drug Delivery Rev.* **2017,** *121*, 133-146.
5. Kozyra, M.; Johansson, I.; Nordling, A.; Ullah, S.; Lauschke, V. M.; Ingelman-Sundberg, M., Human hepatic 3D spheroids as a model for steatosis and insulin resistance. *Sci. Rep.* **2018,** *8* (1), 14297.
6. Stampar, M.; Zabkar, S.; Filipic, M.; Zegura, B., HepG2 spheroids as a biosensor-like cell-based system for (geno)toxicity assessment. *Chemosphere* **2022,** *291* (Pt 1), 132805.
7. Jamieson, L. E.; Harrison, D. J.; Campbell, C. J., Chemical analysis of multicellular tumour spheroids. *Analyst* **2015,** *140* (12), 3910-20.
8. Costa, E. C.; Moreira, A. F.; de Melo-Diogo, D.; Gaspar, V. M.; Carvalho, M. P.; Correia, I. J., 3D tumor spheroids: an overview on the tools and techniques used for their analysis. *Biotechol. Adv.* **2016,** *34* (8), 1427-1441.
9. Saiki, R. K.; Scharf, S.; Faloona, F.; Mullis, K. B.; Horn, G. T.; Erlich, H. A.; Arnheim, N., Enzymatic amplification of β-globin genomic sequences and restriction site analysis for diagnosis of sickle cell anemia. *Science* **1985,** *230* (4732), 1350-1354.
10. Noonan, K. E.; Beck, C.; Holzmayer, T. A.; Chin, J. E.; Wunder, J. S.; Andrulis, I. L.; Gazdar, A. F.; Willman, C. L.; Griffith, B.; Von Hoff, D. D., Quantitative analysis of MDR1 (multidrug resistance) gene expression in human tumors by polymerase chain reaction. *Proc. Natl. Acad. Sci. U.S.A.* **1990,** *87* (18), 7160-7164.
11. Singh, N. P.; McCoy, M. T.; Tice, R. R.; Schneider, E. L., A simple technique for quantitation of low levels of DNA damage in individual cells. *Exp. Cell Res.* **1988,** *175* (1), 184-191.
12. Olive, P. L.; Banáth, J. P.; Durand, R. E., Heterogeneity in radiation-induced DNA damage and repair in tumor and normal cells measured using the" comet" assay. *Radiat. Res.* **1990,** *122* (1), 86-94.
13. Voie, A. H.; Burns, D. H.; Spelman, F. A., Orthogonal-plane fluorescence optical sectioning: Three-dimensional imaging of macroscopic biological specimens. *J. microsc.* **1993,** *170* (3), 229-236.
14. Mosmann, T., Rapid colorimetric assay for cellular growth and survival: application to proliferation and cytotoxicity assays. *J. Immunol. Methods* **1983,** *65* (1-2), 55-63.
15. Liu, B.; Rotenberg, S. A.; Mirkin, M. V., Scanning electrochemical microscopy of living cells: Different redox activities of nonmetastatic and metastatic human breast cells. *Proc. Natl. Acad. Sci. U.S.A.* **2000,** *97* (18), 9855-9860.
16. Torisawa, Y.-s.; Takagi, A.; Shiku, H.; Yasukawa, T.; Matsue, T., A multicellular spheroid-based drug sensitivity test by scanning electrochemical microscopy. *Oncol. Rep.* **2005,** *13* (6), 1107-1112.
17. Dodo, K.; Fujita, K.; Sodeoka, M., Raman Spectroscopy for Chemical Biology Research. *J. Am. Chem. Soc.* **2022,** *144* (43), 19651-19667.
18. Charwat, V.; Schutze, K.; Holnthoner, W.; Lavrentieva, A.; Gangnus, R.; Hofbauer, P.; Hoffmann, C.; Angres, B.; Kasper, C., Potential and limitations of microscopy and Raman spectroscopy for live-cell analysis of 3D cell cultures. *J. Biotechol.* **2015,** *205*, 70-81.
19. Krafft, C.; Schmitt, M.; Schie, I. W.; Cialla-May, D.; Matthaus, C.; Bocklitz, T.; Popp, J., Label-Free Molecular Imaging of Biological Cells and Tissues by Linear and Nonlinear Raman Spectroscopic Approaches. *Angew. Chem., Int. Ed. Engl.* **2017,** *56* (16), 4392-4430.
20. Butler, H. J.; Ashton, L.; Bird, B.; Cinque, G.; Curtis, K.; Dorney, J.; Esmonde-White, K.; Fullwood, N. J.; Gardner, B.; Martin-Hirsch, P. L.; Walsh, M. J.; McAinsh, M. R.; Stone, N.; Martin, F. L. Using Raman spectroscopy to characterize biological materials. *Nat. Protoc.* **2016**, *11*, 664-87.
21. Li, M.; Liao, H. X.; Bando, K.; Nawa, Y.; Fujita, S.; Fujita, K., Label-Free Monitoring of Drug-Induced Cytotoxicity and Its Molecular Fingerprint by Live-Cell Raman and Autofluorescence Imaging. *Anal. Chem.* **2022,** *94* (28), 10019-10026.
22. Xu, N.; Zhu, P.; Liang, J.; Liu, L.; Zhang, W.; Li, X.; He, Y., Label-free Raman spectroscopy monitoring of cytotoxic response induced by a telomerase inhibitor. *Sens. Actuators B,* **2019,** *293*, 1-

10.
23. Kumamoto, Y.; Harada, Y.; Takamatsu, T.; Tanaka, H., Label-free Molecular Imaging and Analysis by Raman Spectroscopy. *Acta. Histochem. Cytochem.* **2018,** *51* (3), 101-110.
24. Majzner, K.; Kochan, K.; Kachamakova-Trojanowska, N.; Maslak, E.; Chlopicki, S.; Baranska, M., Raman imaging providing insights into chemical composition of lipid droplets of different size and origin: in hepatocytes and endothelium. *Anal. Chem.* **2014,** *86* (13), 6666-74.
25. Pettinato, G.; Coughlan, M. F.; Zhang, X.; Chen, L.; Khan, U.; Glyavina, M.; Sheil, C. J.; Upputuri, P. K.; Zakharov, Y. N.; Vitkin, E., Spectroscopic label-free microscopy of changes in live cell chromatin and biochemical composition in transplantable organoids. *Sci. Adv.* **2021,** *7*
26. Bando, K.; Yabuuchi, S.; Li, M.; Kubo, T.; Oketani, R.; Smith, N. I.; Fujita, K., Bessel-beam illumination Raman microscopy. *Biomed. Opt. Express* **2022,** *13* (6), 3161-3170.
27. Jamieson, L. E.; Harrison, D. J.; Campbell, C. J., Raman spectroscopy investigation of biochemical changes in tumor spheroids with aging and after treatment with staurosporine. *J. Biophotonics* **2019,** *12* (5), e201800201.
28. Kim, H.; Han, Y.; Suhito, I. R.; Choi, Y.; Kwon, M.; Son, H.; Kim, H. R.; Kim, T. H., Raman Spectroscopy-Based 3D Analysis of Odontogenic Differentiation of Human Dental Pulp Stem Cell Spheroids. *Anal. Chem.* **2021,** *93* (29), 9995-10004.
29. Jung, N.; Moreth, T.; Stelzer, E. H. K.; Pampaloni, F.; Windbergs, M., Non-invasive analysis of pancreas organoids in synthetic hydrogels defines material-cell interactions and luminal composition. *Biomater. Sci.* **2021,** *9* (16), 5415-5426.
30. Zeng, W.; Guo, L.; Xu, S.; Chen, J.; Zhou, J., High-Throughput Screening Technology in Industrial Biotechnology. *Trends Biotechnol.* **2020,** *38* (8), 888-906.
31. Macarron, R.; Banks, M. N.; Bojanic, D.; Burns, D. J.; Cirovic, D. A.; Garyantes, T.; Green, D. V. S.; Hertzberg, R. P.; Janzen, W. P.; Paslay, J. W., Impact of high-throughput screening in biomedical research. *Nat. Rev. Drug Discovery* **2011,** *10* (3), 188-195.
32. Hirschhaeuser, F.; Menne, H.; Dittfeld, C.; West, J.; Mueller-Klieser, W.; Kunz-Schughart, L. A., Multicellular tumor spheroids: an underestimated tool is catching up again. *J. Biotechol.* **2010,** *148* (1), 3-15.
33. Russell, S.; Wojtkowiak, J.; Neilson, A.; Gillies, R. J., Metabolic Profiling of healthy and cancerous tissues in 2D and 3D. *Sci. Rep.* **2017,** *7* (1), 15285.
34. Kawagoe, H.; Ando, J.; Asanuma, M.; Dodo, K.; Miyano, T.; Ueda, H.; Sodeoka, M.; Fujita, K., Multiwell Raman plate reader for high-throughput biochemical screening. *Sci. Rep.* **2021,** *11* (1), 15742.
35. Wolf, S.; Domes, R.; Merian, A.; Domes, C.; Frosch, T., Parallelized Raman Difference Spectroscopy for the Investigation of Chemical Interactions. *Anal. Chem.* **2022,** *94* (29), 10346-10354.
36. Wolf, S.; Popp, J.; Frosch, T., Multifocal hyperspectral Raman imaging setup for multi-well plates. *Sens. Actuators B* **2022**, 132949.
37. O'Brien, L. E.; Timmins, P.; Williams, A. C.; York, P., Use of in situ FT-Raman spectroscopy to study the kinetics of the transformation of carbamazepine polymorphs. *J. Pharm. Biomed. Anal.* **2004,** *36* (2), 335-40.
38. Czernicki, W.; Baranska, M., Carbamazepine polymorphs: Theoretical and experimental vibrational spectroscopy studies. *Vib. Spectrosc.* **2013,** *65*, 12-23.
39. Braun, D. E.; Maas, S. G.; Zencirci, N.; Langes, C.; Urbanetz, N. A.; Griesser, U. J., Simultaneous quantitative analysis of ternary mixtures of D-mannitol polymorphs by FT-Raman spectroscopy and multivariate calibration models. *Int. J. Pharm.* **2010,** *385* (1-2), 29-36.
40. Burger, A.; Henck, J.-O.; Hetz, S.; Rollinger, J. M.; Weissnicht, A. A.; Stöttner, H., Energy/Temperature Diagram and Compression Behavior of the Polymorphs of d-Mannitol. *J. Pharm. Sci.* **2000,** *89* (4), 457-468.
41. Taylor, L. S.; Zografi, G., Spectroscopic characterization of interactions between PVP and indomethacin in amorphous molecular dispersions. *Pharm. Res.* **1997,** *14* (12), 1691-1698.
42. Jabeen, S.; Dines, T. J.; Leharne, S. A.; Chowdhry, B. Z., Raman and IR spectroscopic studies of fenamates-conformational differences in polymorphs of flufenamic acid, mefenamic acid and tolfenamic acid. *Spectrochim. Acta. A Mol. Biomol. Spectrosc.* **2012,** *96*, 972-85.
43. Hollstein, U., Actinomycin. Chemistry and mechanism of action. *Chem. Rev.* **1974,** *74* (6), 625-652.
44. Hu, S.; Morris, I. K.; Singh, J. P.; Smith, K. M.; Spiro, T. G., Complete assignment of

cytochrome c resonance Raman spectra via enzymic reconstitution with isotopically labeled hemes. *J. Am. Chem. Soc.* **1993,** *115* (26), 12446-12458.
45. Okada, M.; Smith, N. I.; Palonpon, A. F.; Endo, H.; Kawata, S.; Sodeoka, M.; Fujita, K., Label-free Raman observation of cytochrome c dynamics during apoptosis. *Proc. Natl. Acad. Sci. U.S.A.* **2012,** *109* (1), 28-32.
46. Yao, H.-R.; Liu, J.; Plumeri, D.; Cao, Y.-B.; He, T.; Lin, L.; Li, Y.; Jiang, Y.-Y.; Li, J.; Shang, J., Lipotoxicity in HepG2 cells triggered by free fatty acids. *Am. J. Transl. Res.* **2011,** *3* (3), 284.
47. Helal, K. M.; Taylor, J. N.; Cahyadi, H.; Okajima, A.; Tabata, K.; Itoh, Y.; Tanaka, H.; Fujita, K.; Harada, Y.; Komatsuzaki, T., Raman spectroscopic histology using machine learning for nonalcoholic fatty liver disease. *FEBS Lett.* **2019,** *593* (18), 2535-2544.
48. Yamakoshi, H.; Dodo, K.; Okada, M.; Ando, J.; Palonpon, A.; Fujita, K.; Kawata, S.; Sodeoka, M., Imaging of EdU, an alkyne-tagged cell proliferation probe, by Raman microscopy. *J. Am. Chem. Soc.* **2011,** *133* (16), 6102-5.
49. van Manen, H.-J.; Lenferink, A.; Otto, C., Noninvasive imaging of protein metabolic labeling in single human cells using stable isotopes and Raman microscopy. *Anal. Chem.* **2008,** *80* (24), 9576-9582.
50. Ando, J.; Asanuma, M.; Dodo, K.; Yamakoshi, H.; Kawata, S.; Fujita, K.; Sodeoka, M., Alkyne-tag SERS screening and identification of small-molecule-binding sites in protein. *J. Am. Chem. Soc.* **2016**, *138* (42), 13901-13910.